Morphological integration of the human brain across adolescence and adulthood

Ajay Nadig[a,b,1], Jakob Seidlitz[b,c,d], Cassidy L. McDermott[b,e], Siyuan Liu[b], Richard Bethlehem[f], Tyler M. Moore[c,d], Travis T. Mallard[g], Liv S. Clasen[b], Jonathan D. Blumenthal[b], François Lalonde[b], Ruben C. Gur[c,d], Raquel E. Gur[c,d], Edward T. Bullmore[f,h], Theodore D. Satterthwaite[d], and Armin Raznahan[b]

[a]Harvard/MIT MD-PhD Program, Harvard Medical School, Boston, MA, 02115; [b]Section on Developmental Neurogenomics, National Institute of Mental Health, Bethesda, MD, 20892; [c]Department of Child and Adolescent Psychiatry and Behavioral Science, Children's Hospital of Philadelphia, Philadelphia, PA, 19104; [d]Department of Psychiatry, University of Pennsylvania, Philadelphia, PA, 19104; [e]Department of Psychology, University of Pennsylvania, Philadelphia, PA, 19104; [f]Department of Psychiatry, University of Cambridge, Cambridge CB2 1TN, United Kingdom; [g]Department of Psychology, University of Texas at Austin, Austin, TX, 78712; and [h]Cambridgeshire and Peterborough NHS Foundation Trust, Cambridge CB2 1TN, United Kingdom

Edited by Marcus E. Raichle, Washington University in St. Louis, St. Louis, MO, and approved February 24, 2021 (received for review November 25, 2020)

Brain structural covariance norms capture the coordination of neurodevelopmental programs between different brain regions. We develop and apply anatomical imbalance mapping (AIM), a method to measure and model individual deviations from these norms, to provide a lifespan map of morphological integration in the human cortex. In cross-sectional and longitudinal data, analysis of whole-brain average anatomical imbalance reveals a reproducible tightening of structural covariance by age 25 y, which loosens after the seventh decade of life. Anatomical imbalance change in development and in aging is greatest in the association cortex and least in the sensorimotor cortex. Finally, we show that interindividual variation in whole-brain average anatomical imbalance is positively correlated with a marker of human prenatal stress (birthweight disparity between monozygotic twins) and negatively correlated with general cognitive ability. This work provides methods and empirical insights to advance our understanding of coordinated anatomical organization of the human brain and its interindividual variation.

cerebral cortex | development | lifespan

Across the cortical sheet, communities of brain regions covary in morphological features such as cortical thickness or volume; this phenomenon is referred to as structural covariance (1). Structural covariance can arise from morphological integration, where the anatomy of different brain regions is shaped by shared developmental processes. In particular, if the same developmental program shapes the morphology of different brain regions, we would expect those brain regions to covary across individuals in a population where there is variation in that shared developmental program (2). Consequently, the degree to which a given individual deviates from population-level structural covariation in the brain could provide a powerful indicator of how faithfully that individual has enacted the layered developmental programs (3) that underpin human neuroanatomical variation. However, although the study of individual deviations from anatomical covariance norms has a long and successful history in research on nonhuman animals (3)—particularly in the case of deviations from bilateral symmetry ("fluctuating asymmetry") (4)—there has been a relative lag in their application to human data. This gap is particularly striking given the increasingly rich and spatiotemporally dense morphometric data sets provided by modern magnetic resonance imaging (MRI) of the living human brain (5). Here, to close this gap, we introduce and apply anatomical imbalance mapping (AIM), a method that provides person-level estimates of both global and interregional deviations from structural covariation norms.

We use AIM to characterize spatiotemporal patterning of anatomical imbalance in the human brain within a primary cross-sectional neuroimaging data set of 185 structural MRI scans from healthy youth aged 6 through 25 y and then replicate these developmental findings in an overlapping sample of individuals with longitudinal scans (648 scans from 399 participants). Studying participants in this age range allows us to evaluate time-varying anatomical imbalance and thereby delineate the integration of neurodevelopmental processes that are active in this critical etiological time window for neuropsychiatric disease (6–8). In particular, we seek to assess whether anatomical imbalance is developmentally dynamic (i.e., whether individuals change in their distance from population covariance over time). To further assess the robustness and reproducibility of our findings, we pursue a similar analysis in three independent developmental neuroimaging data sets. Next, to test for dynamism of anatomical imbalance across the human lifespan, we extend AIM to analyze three further data sets, which in combination with our developmental data sets include scans from 21,711 individuals from 6 to 87 y of age. In particular—motivated by the growing consensus that developmental and aging processes act on shared neural substrates (9–11)—we use this expanded lifespan data set to ask whether and how developmental changes in anatomical imbalance are "mirrored" in typical aging. Finally, to address the notion that interindividual variation in anatomical

Significance

Attaining correct anatomical proportions is an important developmental goal. Although the patterning of individual deviations from such proportions has been well-studied in nonhuman animals and various human body measurements, this theoretical framework has not been applied to human brain morphology. We analyze individual deviations from proportionality norms ("anatomical imbalance") in a collection of over 20,000 brain MRI scans to reveal that individuals grow closer to proportionality norms in development and further from proportionality norms in aging. This effect is greatest in brain networks that support higher-order cognition and least in brain networks that support sensorimotor functions. We demonstrate that deviation from proportionality norms—a measure of neurodevelopmental coordination—is associated with cognitive function and sensitive to variation in prenatal stress.

Author contributions: A.N. and A.R. designed research; A.N., J.S., C.L.M., L.S.C., J.D.B., and F.L. performed research; S.L., R.B., T.M.M., T.T.M., R.C.G., R.E.G., E.T.B., and T.D.S. contributed new reagents/analytic tools; A.N., J.S., S.L., R.B., T.M.M., T.T.M., and F.L. analyzed data; and A.N., J.S., and A.R. wrote the paper.

The authors declare no competing interest.

This article is a PNAS Direct Submission.

[1]To whom correspondence may be addressed. Email: ajay_nadig@hms.harvard.edu.

This article contains supporting information online at https://www.pnas.org/lookup/suppl/doi:10.1073/pnas.2023860118/-/DCSupplemental.

Published April 1, 2021.

imbalance may serve as a proxy for developmental instability (12), we relate interindividual variation in anatomical imbalance to independent measures of 1) developmental stress, as captured by birthweight disparity between monozygotic twins, and 2) intelligence quotient (IQ), which has previously been associated with fluctuating asymmetry (13).

Results

AIM takes advantage of well-characterized population-level anatomical covariance within the human brain (1) to estimate an individual's deviation from norms of coordinated morphological development. A particularly well-studied aspect of structural covariance is the phenomenon of interregional correlations in thickness of the cerebral cortex. Patterns of cortical thickness covariance in humans are highly reproducible and heritable (14). These covariance patterns have also been linked to variations in rates of anatomical change over development, interregional coordination of brain activity and gene expression (15–19), and interindividual variation in cognitive ability (20). Furthermore, several neurodevelopmental and neurodegenerative diseases are associated with disruptions of normative structural covariance (21–24). We therefore used interregional cortical thickness covariances as the normative reference from which to calculate individual-level interregional anatomical imbalance scores (Fig. 1 and *Materials and Methods*).

To assess basic properties and replicability of AIM, we computed anatomical imbalance in a core cross-sectional sample of unrelated individuals (NIH Study of Healthy Brain Development, $n = 185$). All scans had an average (left and right) Euler number (a quantitative quality assessment metric) less than 217; this threshold has been demonstrated to successfully identify low-quality scans with high sensitivity (25). We calculated structural covariance norms using regionwise cortical thickness estimates that were residualized for age, sex, and Euler number. Each individual was scored for their deviation from these norms between all pairs of cortical regions (Fig. 1)—capturing their anatomical imbalance for each region pair as compared to the balancing of regional dimensions expected from population covariance norms. Any scan whose global average anatomical imbalance (i.e., average across all pairs of regions) was further than 4 SDs from the cohort mean was excluded. We confirmed that these quality control procedures effectively controlled for noise due to subject motion and registration error (*SI Appendix*).

To visualize anatomical imbalance across the cortical sheet, we collapsed pairwise interregional imbalance estimates into a measure of average unsigned anatomical imbalance for each brain region per person. A group-level average of these individual maps revealed that the regions in the lowest 5% of anatomical imbalance were the bilateral caudal middle frontal gyrus, bilateral pars opercularis, bilateral pericalcarine gyrus, bilateral postcentral gyrus, left supramarginal gyrus, right paracentral gyrus, and right precentral gyrus (Fig. 1*E*). The regions in the highest 5% of anatomical imbalance were the bilateral entorhinal cortex, bilateral inferior temporal gyrus, bilateral parahippocampal gyrus, bilateral superior temporal gyrus, bilateral frontal pole, bilateral temporal pole, right fusiform gyrus, and right middle temporal gyrus (Fig. 1*E*). Regional variation in mean anatomical imbalance was inversely related to regional variation in mean structural covariance (*SI Appendix*, Fig. S1) and highly reproducible between our primary NIH sample and three independent cross-sectional samples: healthy controls from the Autism Brain Imaging Data Exchange (ABIDE), $n = 313$; Philadelphia Neurodevelopmental Cohort (PNC), $n = 1168$; and NeuroScience in Psychiatry Network (NSPN), $n = 291$ (mean intercohort correlations: $r > 0.73$ for mean imbalance across brain regions, $r > 0.66$ for imbalance across region pairs). In order to ensure comparability between the ABIDE data set and the other developmental cohorts, we subset the ABIDE data set to individuals under the age of 25, matching the age ceiling of the other developmental cohorts. Structural covariance norms were calculated separately for each data set.

Anatomical Imbalance Declines across Development. Cross-sectional analysis within our primary NIH data set indicated that greater age was associated with less global anatomical imbalance (i.e., a lower person-wise mean of all interregional anatomical imbalance estimates, Fig. 2*A*, $r = -0.37$, $P < 0.001$). We replicated this linear decrease of global anatomical imbalance over development in the PNC (Fig. 2*A*, $r = -0.41$, $P < 0.001$), ABIDE (Fig. 2*A*, $r = -0.35$, $P < 0.001$) and NSPN (Fig. 2*A*, $r = -0.17$, $P = 0.001$) data sets We confirmed that the observed decline in

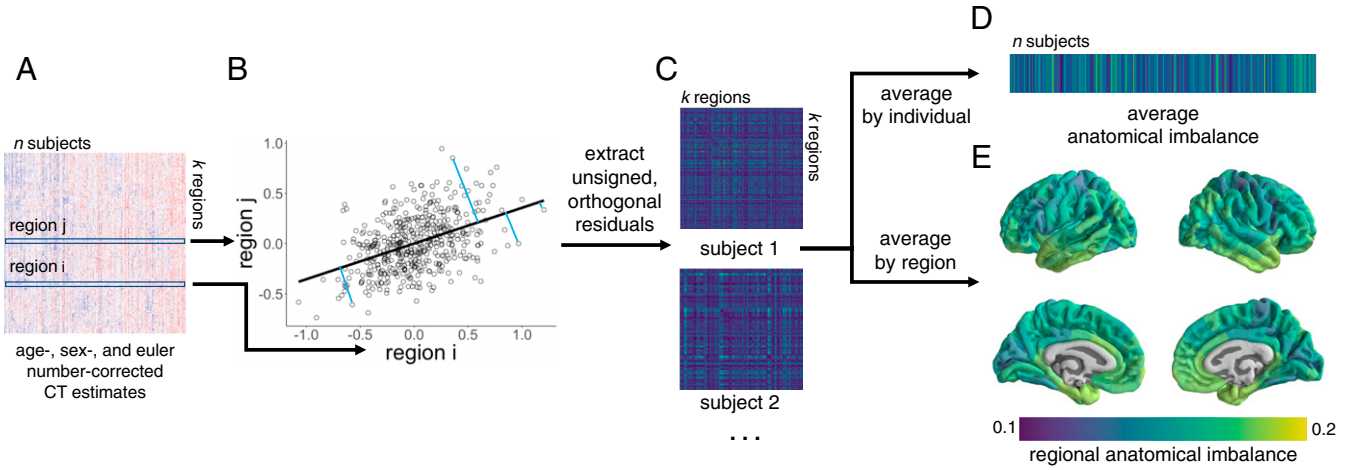

Fig. 1. Workflow for AIM. (*A*) First, we estimate cortical thickness at *k* regions across the cortex in each subject, regressed for age, sex, and Euler number. (*B*) We then create a linear model relating cortical thickness between pairs of regions and extract orthogonal residuals from those fits (examples shown in teal). (*C*) This gives a symmetric *k* regions × *k* regions matrix for each individual, where values are orthogonal distance from covariance norms (i.e., anatomical imbalance) for each pair of regions. (*D*) These anatomical imbalance estimates can be averaged across all pairs of regions (i.e., the upper or lower triangle of matrices depicted in *C*) to give a summary estimate of anatomical imbalance per individual. (*E*) Anatomical imbalance estimates can also be averaged by region, giving a cortical map of average anatomical imbalance, which is displayed here for the cross-sectional NIH data set.

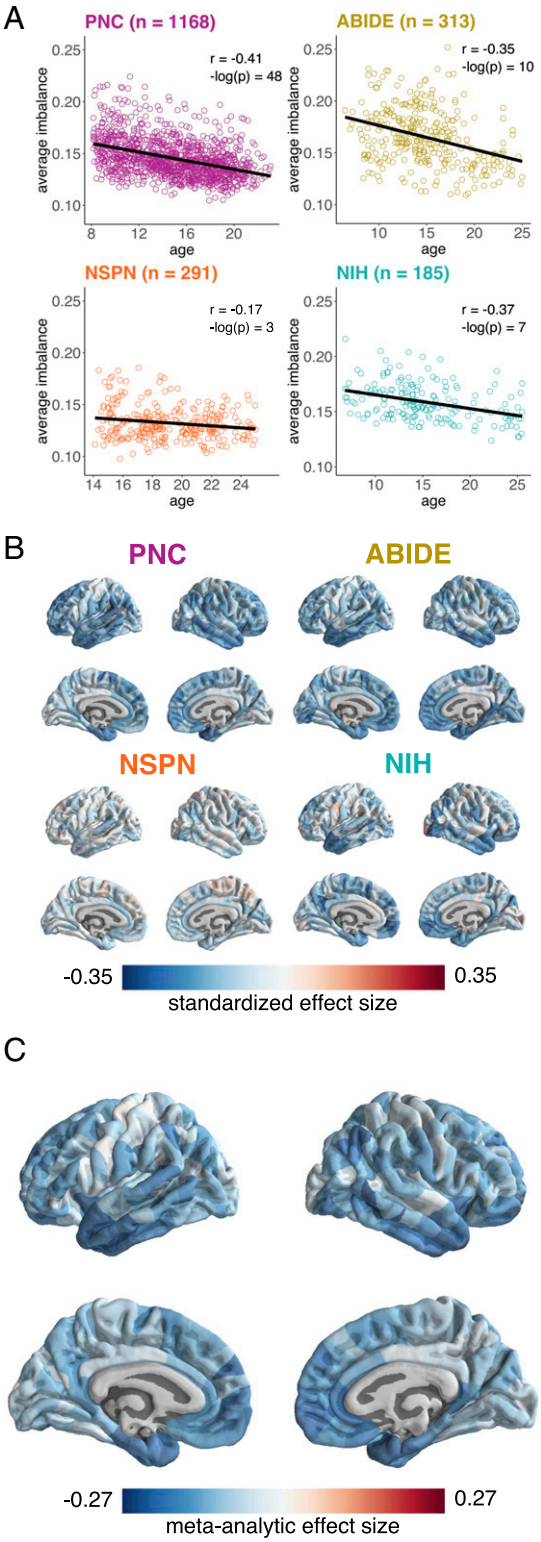

Fig. 2. Anatomical imbalance declines across development. (*A*) Decline in global anatomical imbalance across development in four developmental data sets. Each point is a unique individual. (*B*) Cortical maps of imbalance decline (quantified as the coefficient from a model regressing *z*-scored age on *z*-scored average regional imbalance) for each data set. Spatial correlations with NIH map: $r_{NIH,PNC} = 0.38$, $r_{NIH,ABIDE} = 0.34$, and $r_{NIH,\ NSPN} = 0.15$. (*C*) Cortical map of fixed effects, inverse variance weighted meta-analytic effect sizes for the effect of age on regional anatomical imbalance, computed from the four maps in *B*.

anatomical imbalance with age does not arise from changing covariance structure over development (*SI Appendix*).

The rate of this developmental age-related decrease in anatomical imbalance varied markedly across the cortical sheet (Fig. 2*B*). The spatial patterning of age effects on anatomical imbalance in the primary NIH data set was modestly reproducible in all three independent cross-sectional replication data sets (Fig. 2*B* and *SI Appendix*, Fig. S2; correlation in regional age effects: $r_{NIH,\ PNC} = 0.38$, $r_{NIH,\ ABIDE} = 0.34$, $r_{NIH,\ NSPN} = 0.15$). The observed spatial similarity between data sets in age effects on anatomical imbalance was statistically significant relative to empirical null distributions generated by random spatial rotations of the NIH age effects map [$p_{spin:\ NIH,PNC} < 0.001$, $p_{spin:\ NIH,ABIDE} < 0.001$, $p_{spin:\ NIH,NSPN} = 0.015$, *SI Appendix*, Fig. S2 and *Materials and Methods* (6, 26)]. Of note, the effects of age on both global and regional anatomical imbalance from cross-sectional analyses in the NIH data set could be replicated using longitudinally acquired scans that were available for an overlapping set of individuals (648 scans from 399 individuals, *SI Appendix*, Fig. S2). To synthesize the four cross-sectional age-effect maps into a single consensus map, we performed a fixed-effects, inverse-variance-weighted meta-analysis at each region (Fig. 2*C*). A large proportion of regions show developmental decreases in mean anatomical imbalance (140/308 regions showed statistically significant decline of anatomical imbalance over development after Bonferroni correction for multiple comparisons).

Taken together, these findings indicate that regional patterning of cortical thickness becomes less individualized over development and that the rate of this convergence to population norms varies in a highly reproducible manner across the cortical sheet. In other words, we find that the human cortical sheet shows a "tightening" of morphological integration between childhood and adolescence, which proceeds at different rates for different cortical regions.

Declining Anatomical Imbalance with Age Varies among Functional Cortical Networks. Given the highly stereotyped regional patterning of age effects on anatomical imbalance (Fig. 2), we next asked whether regional differences in age-related anatomical imbalance change over development are organized by known functional properties of the cortical sheet. To answer this question, we developed a simple framework for testing enrichment of a continuous cortical map in discrete cortical parcels, where enrichment is quantified as the proportion of brain-wide signal in each network divided by the size of each network (*Materials and Methods*). Using the meta-analytic developmental age effect map (Fig. 2*C*), we computed the enrichment of age-related anatomical imbalance over development change in each of the seven canonical functional networks defined by Yeo, Krienen et al. (27) (Fig. 3*A*) and compared these values against null distributions generated by spatially permuting the standardized effect size map (rotationally) and recomputing enrichment 10,000 times. This procedure revealed that rapid developmental age-related reductions in anatomical imbalance were significantly greater than null expectation within the default mode (enrichment = 1.2, $P = 0.008$) and limbic networks (enrichment = 1.6, $P < 0.001$) and significantly less than null expectation in the somatomotor network (enrichment = 0.73, $P = 0.009$) (Fig. 3*B*). We additionally assessed and verified (Fig. 3*D*) that these internetwork differences in anatomical imbalance reduction over development could be explained by internetwork differences in intercept from the same model (i.e., the theoretical "starting" anatomical imbalance value). Thus, tightening of morphological integration within the human cortex appears to vary in pace between different functional networks: Lower-order systems already show strong morphological integration in early childhood, with little subsequent developmental change, whereas the

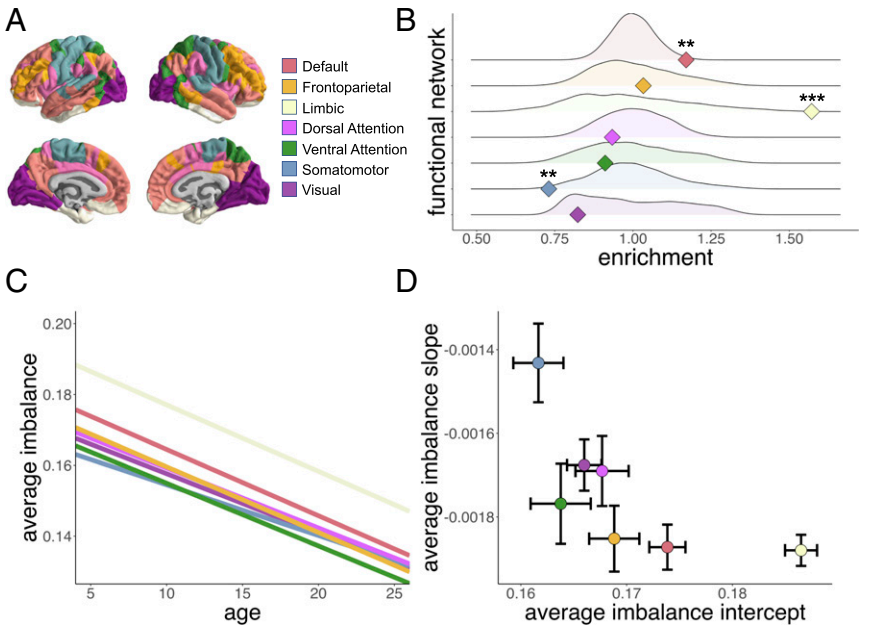

Fig. 3. Anatomical imbalance decline is patterned across functional networks. (*A*) Functional networks of Yeo, Krienen et al. (27). (*B*) Testing for significant enrichment of anatomical imbalance decline with development in each functional network against a null distribution generated by "spin"-based spatial permutation of the meta-analytic age/imbalance effect map (Fig. 2*C*, *Materials and Methods*, $^{**}P < 0.01$, $^{***}P < 0.001$). (*C*) Age effects on anatomical imbalance for each functional network. (*D*) Relationship between slopes and intercepts of fits from *C* (with intercept referring to value at age 5 y). We show point estimates (dots) and SEM across regions in each network (lines) for slope and intercept coefficients.

process of morphological integration is more protracted in higher-order systems.

Lifespan Analysis of Anatomical Imbalance Reveals Mirrored Processes in Development and Aging. To extend our developmental findings into later ages, we implemented AIM in three additional data sets: the Human Connectome Project (HCP; n = 448), the UK BioBank (UKB; n = 18,732), and the Cambridge Center for Aging and Neuroscience repository (Cam-CAN; n = 516). Additionally, we made use of the full set of controls from the ABIDE data set (n = 367, i.e., now including individuals over 25 y of age). We harmonized these data sets, as well as the other developmental data sets (Fig. 2), using ComBAT (28) (*Materials and Methods*). Spline modeling (*Materials and Methods*) across the harmonized data set revealed a significant effect of age (F = 68, −log(p) = 111), such that global anatomical imbalance reduces rapidly over development, largely stabilizes in early adulthood (after ∼25 y of age), and then increases sharply with advancing age beyond the seventh decade of life (Fig. 4*A*). The effect of age remained highly significant after including sex, Euler number, and cohort as covariates (F = 50, −log(p) = 75).

We next modeled the relationship between age and average anatomical imbalance in each adult data set separately. We found no relationship between average imbalance and age in the HCP data set (age range: 22 to 36 y, r = 0.02, P = 0.64). In the UKB data set, we found a small but highly significant increase in average imbalance with age (age range: 44 to 80 y, r = 0.07, −log(p) = 23)—reflecting the exceptionally large sample size of this cohort. However, in the full Cam-CAN data set—which notably extends into older age—we observed a significant increase in average imbalance with age (r = 0.41, −log(p) = 22). To assess the topography of aging effects, we subset the Cam-CAN data set to individuals over the age of 50 (n = 269), as has been done previously (29) (Fig. 4*B*). Comparison of the Cam-CAN map of age-related AIM variation with the meta-analytic developmental age-effect maps revealed a weak but statistically significant anticorrelation between the regional patterning of age-related anatomical imbalance variation in aging and in development (Fig. 4*C*; r = −0.21, p_{spin} = 0.020). This finding indicates that the cortical territories with large anatomical imbalance declines in development are more likely to experience large anatomical imbalance increases in aging.

Anatomical Imbalance Is Associated with Functional Outcomes and Is Sensitive to Developmental Stress. Having established that global anatomical imbalance is highly dynamic in development and aging and shows considerable interindividual variation, we next sought to test whether this interindividual variation in anatomical imbalance was related to functional outcomes and developmental stress. We first compared interindividual variation in global anatomical imbalance to variation in general cognitive ability (IQ) as an extensively studied functional outcome metric which has been linked to prior morphological markers of developmental instability (30) and shows good psychometric properties and predictive validity (31). In the core NIH sample and two of our replication data sets that provided comparable IQ measures, we identified a small but consistent negative correlation between global anatomical imbalance (age- and sex-normed) and IQ (Fig. 5*A*; NIH: r = −0.13, P = 0.096; ABIDE: r = −0.15, P = 0.007; NSPN: r = −0.09, P = 0.119). We further assessed and verified agreement between our results and a recent meta-analysis of studies relating fluctuating asymmetry to IQ (13) by meta-analyzing the anatomical imbalance/IQ relationships across all these three data sets (Fig. 5*B*; meta-analytic r = −0.12, $P < 0.001$). Although comparable IQ test data were not available in the other cohorts we analyzed, those cohorts had heterogeneously defined intelligence estimates (HCP and PNC: factor-analysis based estimates, Cam-CAN: Cattell Culture Fair Intelligence Test, UKB: Verbal Numerical Reasoning) that allowed us to probe the reproducibility of the discovered inverse relationship between average anatomical imbalance and general cognitive ability. We observed a significant negative correlation

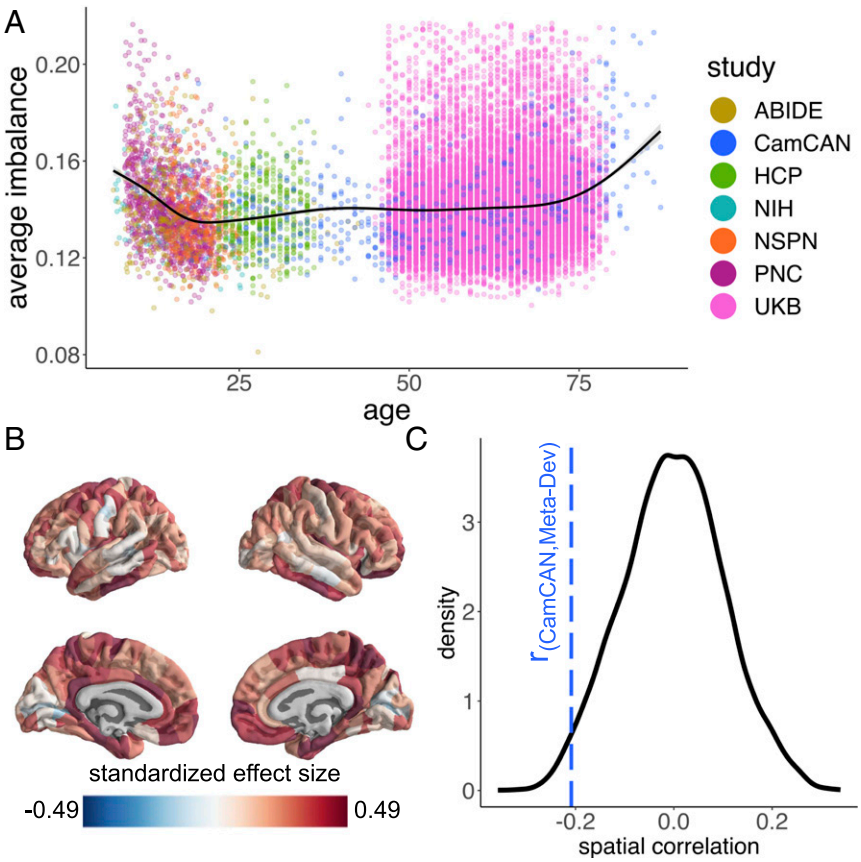

Fig. 4. Anatomical imbalance is dynamic across the lifespan. (*A*) Global anatomical imbalance of 21,711 individuals from seven data sets that tessellate the lifespan. CT estimates were harmonized across cohorts with ComBAT, and the imbalance/age relationship was modeled with smoothing splines. (*B*) Cortical map of imbalance/age standardized effect sizes observed in individuals 50 y of age and older from the Cam-CAN cohort. Standardized effect size was quantified as the coefficient from a model regressing scaled age on scaled average regional imbalance. (*C*) Testing the spatial correlation of anatomical imbalance change between the meta-analytic developmental imbalance/age map (Fig. 1C) and the Cam-CAN imbalance/age map (B) against a null hypothesis generated by a "spin"-based spatial permutation of the meta-analytic developmental map.

between average imbalance and general cognitive ability in each of these four additional data sets (*SI Appendix*, Fig. S4).

We next examined the relationship between global anatomical imbalance and a marker of developmental stress in humans—birthweight differences between monozygotic twins (32). If anatomical imbalance captures variation in early developmental stress, we reasoned that global brain anatomical imbalance should be greater in the lighter versus heavier cotwin. Supporting this prediction, we observed that global anatomical imbalance from brain MRI scans acquired in later childhood (9 to 10 y of age) was modestly but statistically significantly greater in the lighter- versus heavier-born members of 256 monozygotic twin pairs (*Materials and Methods*) from the Adolescent Brain Cognitive Development project (ABCD) (33) (Fig. 5*C*, Cohen's d = 0.15, P = 0.013). This effect persisted after correcting for age, sex, twin pair average Euler number, and twin pair average of a composite cognition score derived from the NIH Toolbox (P = 0.017). Taken together, these findings suggest that interindividual variation in global anatomical imbalance may serve as a functionally relevant marker that captures effects of in utero environmental stress.

Discussion

By introducing AIM and applying it to several large-scale in vivo neuroimaging data sets, our work provides several fresh insights into the patterning of neuroanatomical variation in humans.

First, we find that overall anatomical imbalance within the human brain shows a highly reproducible age-related decline over childhood and adolescence (Fig. 2*A* and *SI Appendix*, Fig. S3) and reaches a minimum at age ~25 y (Fig. 4*A*). These observations imply an overall tightening of morphological integration over human brain development. In other words, despite the various starting points and presumed diversity of genomic and environmental factors in the presently studied individuals, we observe a remarkably consistent tendency toward population covariance norms during development. Thus, the decline in brain anatomical imbalance that we observe over childhood and adolescence from in vivo imaging constitutes a modern example of developmental canalization (12, 34)—a concept first articulated by Conrad Waddington in the mid-20th century (35). Morphological integration of cortical anatomy requires the coordination of developmental processes among brain regions, and such coordination could, for example, be achieved by shared genetic influences on anatomical variation among brain regions (36, 37). In support of this interpretation, we have previously reported a general pattern of increasing genetic correlations between interregional cortical thickness over human development (38). There is also evidence that developmental changes in the genetic correlation between regional cortical thickness may reflect different sources of genetic variation at different developmental stages (39)—in line with the notion of structural covariation as a layering of different components of morphological integration (3). Coordination of anatomical change between brain regions

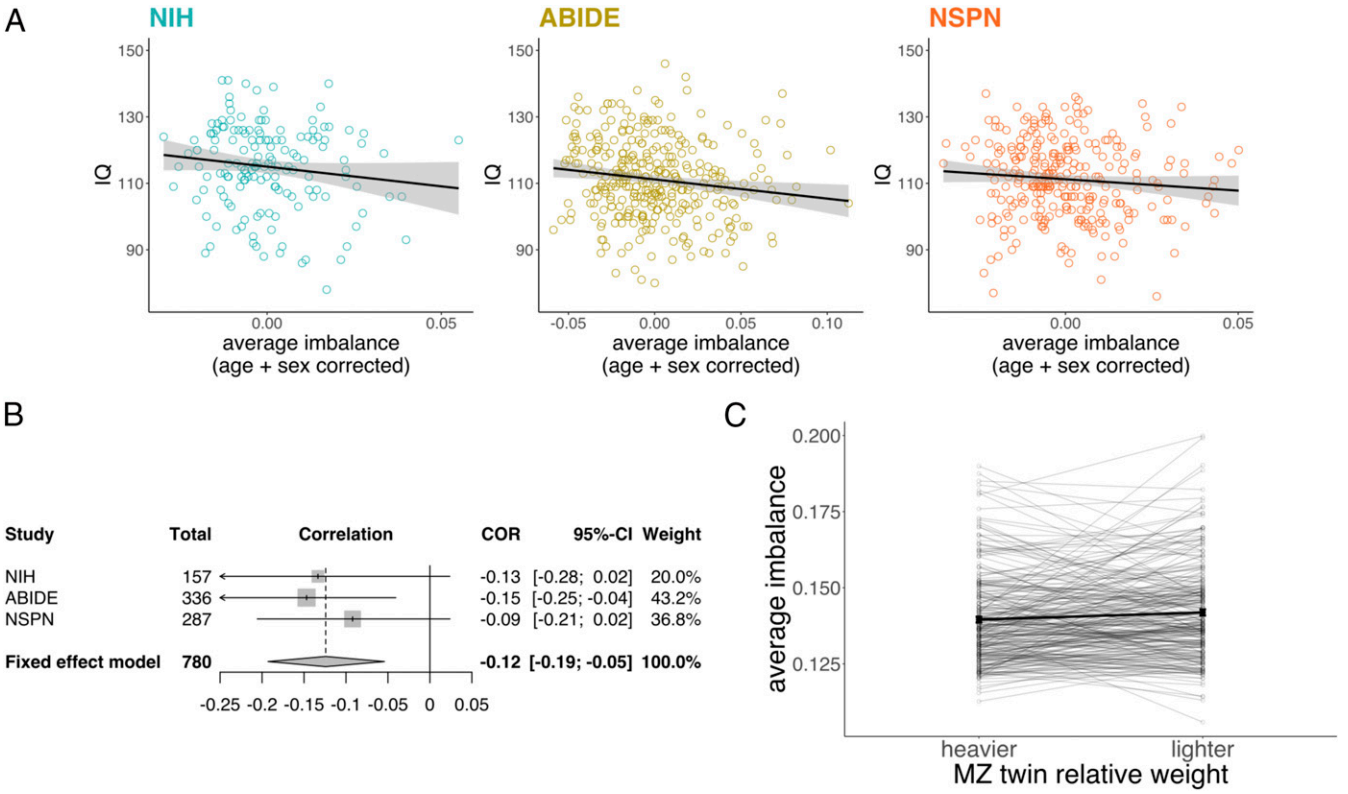

Fig. 5. Individual anatomical imbalance estimates are associated with functional outcomes and subtle developmental insults. (*A*) Relationship between age- and sex-regressed individual anatomical imbalance estimates and full-scale IQ in NIH, ABIDE, and NSPN data sets. (*B*) Meta-analysis of effects from *A*. (*C*) Comparison of individual global anatomical imbalance estimates between heavier and lighter cotwins in the ABCD data set (*Materials and Methods*). Bolded points indicate means for each group.

has also been widely speculated to arise through active trophic effects of coordinated neuronal activation (21). This mechanism is supported by the recent observation that structural covariance is correlated with structural connectivity as measured by tract tracing in mice (18) and suggests that stereotyped and sustained patterns of functional connectivity over development (38) could act as one proximal driver for the age-related increases in morphological integration revealed by AIM.

Second, we find that the rate of morphological integration over development varies greatly among regions of the cortical sheet, and this regional variation is organized by the brain's functional topography. Lower-order sensorimotor cortices show the lowest levels of anatomical imbalance at age 5 y and the least age-related changes in anatomical imbalance over development (Fig. 3). This pattern of earlier structural development in sensorimotor cortex is congruent with previous descriptions of neuroanatomical developmental trajectories (40), providing convergent validity for our method. One interpretation of this observation is that anatomical development of these regions is canalized earlier on in development, congruent with the earlier functional maturation of these cortical systems compared with those that support later-mastered behavioral and cognitive competencies (41). This interpretation is supported by our observation of a strong correlation between slope and intercept of the age-imbalance relationship across functional networks, such that functional networks with the least negative slope have the lowest starting anatomical imbalance. Relative to these lower-order systems, anatomical imbalance is greatest at age 5 y and most developmentally dynamic in limbic and higher-order associative cortices within the brain's "default mode network" (Fig. 3). These more slowly canalizing regions are notable for association with diverse psychopathologies, such as mood and psychotic disorders (42–44). The fact that morphological integration for these networks is still being established between the ages of 5 and 25 y provides a context for known associations between these networks and developmentally emergent mental disorders.

Third, we show that the tightening of morphological integration during human brain development is inverted in a loosening of morphological integration during late aging. These two phases of dynamism are separated by a long period of relative stability in the brain's morphological organization (at least through the lens of cortical thickness) between ~25 and 60 y of age. This finding suggests that the most developmentally dynamic neural systems are also the most vulnerable to aging-related change. Thus, our findings are consistent with a "last-in, first-out" model, where the latest functional networks to develop are those that show the most precipitous decline in aging (9, 10, 45). The inflection toward age-related increases in AIM in the seventh decade of life after a period of relative stability may reflect an age-related shift in the genetic programs regulating variation in brain anatomy (46). Intriguingly, it has also recently been shown that a core spatial pattern of genetic influences on human cortical thickness variability appears to organize the spatial patterning of cortical thickness change in development as well as aging (29). This observation provides a potential explanation for the partial congruence between age-related differences in regional AIM across both development and aging. Our finding that age-related AIM increases in aging are most pronounced over medial temporal cortices raises the possibility that interindividual variability in AIM within these regions may correlate with interindividual variability in risk for neurodegenerative disorders such as Alzheimer disease that have been associated with these very regions of the brain (47). Thus, an important goal for future work will be

to determine if interindividual variation in the rate of anatomical imbalance change in development and aging might relate to variation in neurodevelopmental and neurodegenerative clinical outcomes, respectively.

Fourth, we relate individual anatomical imbalance estimates to both functional outcome and developmental insult. We find that across three independent data sets that vary substantially in ascertainment and scanning protocol, global brain anatomical imbalance is weakly, but consistently, correlated with IQ. The effect size of this relationship is identical to that of a recent meta-analysis of the relationship between fluctuating asymmetry and intelligence (13). Critically, we do not suggest that anatomical imbalance is a good predictor for intelligence and only conclude that 1) the imbalance–intelligence relationship is consistent, and 2) the variance in intelligence captured by anatomical imbalance is concordant with the variance in intelligence captured by the best-studied marker of developmental instability to date. Encouragingly, these conclusions align with those of a prior report that predicted IQ using a distinct "leave one out" procedure for estimating individual contribution to structural covariance (48).

To explore the effect of developmental stress on anatomical imbalance, we used a unique collection of MRI scans from twins aged 9 to 10 y from the ABCD cohort (33) and found that subtle differences in birthweight between cotwins precipitate mild differences in anatomical imbalance, such that the lighter twin has slightly higher imbalance. Low birthweight is associated with adolescent- and adult-onset psychiatric disorders (49) and is affected by various intrauterine factors such as blood pressure and degree of insulin signaling (50). Our findings suggest that exposure to more prenatal environmental stress (as indicated by the proxy of birthweight differences between monozygotic twins) weakens brain morphological integration as measured later in life, likely reflecting disruption of coordinated neurodevelopmental programs.

The biological insights discussed above stem in part from those methodological aspects of AIM analysis that distinguish it from prior approaches for structural covariation analysis in the developing human brain (6–8). Most fundamentally, AIM is distinct from these prior approaches for its focus on individual-level deviations from anatomical covariance norms rather than the magnitude of group-level anatomical covariance itself. Through this distinction, AIM provides individual-level trait measures for morphological integration that allow rich and flexible comparisons with any individual-level demographic, genetic, cognitive, behavioral, or clinical features of interest. We therefore see AIM as a complementary tool to structural covariance analysis for understanding the patterning of anatomical variability within the brain. There are several lines of empirical evidence that support this point of view. First, while there are some developmental phenomena that both methods recover [e.g., earlier maturation of sensorimotor versus associative systems (7, 19), stabilization of anatomical variability in adulthood (6), and a U-shaped pattern across the lifespan (51)], comparison with prior reports (6) and analysis in our current report (*SI Appendix*) indicate that shifts in structural covariance and anatomical imbalance over brain development are dissociable from one another. This dissociation hints at the importance of distinguishing between the following two developmental processes: a shift toward adult-like proportions (i.e., changing covariance relationships) and greater consistency across individuals in proportionality (i.e., decreasing anatomical imbalance). We hypothesize that these two phenomena are the result of a canalized developmental process (12), where more variable younger brains become progressively less variable as they attain adult-like proportions. Put differently, the normative adult covariance pattern is a dynamical attractor (52), which attracts all individual developmental trajectories despite their variable starting points. Similar observations of changing pattern with declining variability have been made in numerous developmental settings, including vulva induction in *Caenorhabditis elegans* (53) and blastoderm segment determination in *Drosophila* (54). Whether and how other neurodevelopmental processes are accompanied by decreases in configurational variability is an intriguing direction for future research.

While we were able to demonstrate that decreasing AIM is independent of changing covariance structure (*SI Appendix*), future work is needed to better understand the biological substrates for this dissociability. Encouragingly, past work has used linear regression approaches to detect distinct age and cognitive associations for the "slope" versus the "scatter" of bivariate morphometric relationships between cortical regions (55), offering a potential analogy to dissociability of developmental findings for structural covariance and AIM. An important goal for future work will be delving further into the nature of this dissociability through comparative analysis of genetic (37), phenotypic (56), and developmental (57) associations.

While we implemented several procedures to check for and remove motion- and registration-related variance from AIM estimates (*Results*, *Materials and Methods*, and *SI Appendix*), a portion of variation in AIM estimates may still relate to cortical thickness misestimation from recalcitrant challenges in neuroimaging such as participant motion or the inability to perfectly align cortical surfaces between different individuals. These challenges remain areas of ongoing work in the field (25, 58, 59), and future advances may be incorporated into AIM.

Taken together, the work presented herein provides several fresh insights into normative development of anatomical coordination in the human brain, and offers a set of tools for dissecting this coordination—both at varying spatiotemporal scales and as a function of interindividual variation in any other trait(s) of interest. Initial application of these tools in the current paper provides a map of how developmental and aging processes are spatiotemporally coordinated in the human brain. We further demonstrate that this coordination is linked to the brain's functional architecture, related to cognitive outcomes, and sensitive to prenatal stress.

Materials and Methods

Informed Consent and Institutional Review Board Approval. All subjects provided informed consent for participation in the cohorts described in this paper. The approving Institutional Review Boards (IRBs) were the NIH IRB, the University of Pennsylvania IRB, the Children's Hospital of Philadelphia IRB, the UK National Research Ethics Service, the Washington University IRB, the UK BioBank Ethics and Guidance Council, the Cambridgeshire 2 Research Ethics Committee. The ABIDE and ABCD data sets include many sites, each with their own IRB procedure; however, IRB approval and informed consent was required for inclusion in these data sets. Detailed information about subject recruitment and IRB approval is presented in *SI Appendix*, Table S2.

MRI Data Acquisition and Preprocessing. Acquisition parameters, preprocessing description, and sample characteristics for each sample are described in *SI Appendix*, Table S1. Cortical surface reconstructions were generated using FreeSurfer version 5.3 (NIH, PNC, ABIDE, NSPN, HCP, Cam-CAN) and version 6.0 (UKB, ABCD) (surfer.nmr.mgh.harvard.edu/) (60–62), which relies on T1-weighted MRI scans (63), includes methods for estimating cortical morphometric measures such as cortical thickness and surface area (64, 65), and performs intersubject alignment via nonlinear, surface-based registration to a population template brain, driven by cortical folding patterns (66). For the longitudinal analysis (*SI Appendix, Supplementary Information Text* and Fig. S3), we used the FreeSurfer longitudinal pipeline (67) as implemented in FreeSurfer version 5.3. For all analyses, we excluded any scan whose left-right mean Euler number exceeded 217, following previously established recommendations (25).

Cortical Parcellation. To define cortical regions for this analysis, the 68 regions of the Desikan-Killany atlas (68) were subdivided into 308 regions of approximately equal size as previously described (69). This asymmetric parcellation was generated on the surface of the Freesurfer standard anatomical

template (fsaverage) and then transformed to each individual subject's surface. Mean CT in each region was calculated across all constituent vertices per region in individual subject surfaces. Cortical thickness was estimated for each region using FreeSurfer (*SI Appendix*, Table S1).

Anatomical Imbalance Mapping. We first regressed FreeSurfer-generated cortical thickness estimates for age, sex, Euler number, with the following linear model:

$$\text{CT} \sim \text{age} * \text{sex} * \text{Euler number}.$$

In the case of the ABIDE data set, which includes many sites, we included site as an additional additive linear covariate. Following all prior primary publications using the NSPN cohort (6, 70), we did not correct for site, as acquisition sequences were identical and empirically shown to have minimal differences between sites (71).

To define structural covariance norms between each pair of cortical regions, we employed a total least squares regression (using the *odregress* function in the R package *pracma*). This procedure minimizes orthogonal distances and provides a fit that is symmetric regardless of which region is entered as the dependent variable. From these pairwise models, we extracted unsigned, orthogonal residuals, which corresponded to individual anatomical imbalance estimates for each pair of regions. These residuals were averaged across all region pairs within an individual to derive a person-level estimate of global anatomical imbalance. We averaged residuals per region to provide a spatial map of regional anatomical imbalance for each individual.

In the present analysis, we have used absolute (i.e., unsigned) residuals to estimate anatomical imbalance. However, the AIM pipeline could be easily modified to quantify signed residuals, thereby retaining information about which region is larger than expected from the size of another region given interregional covariance norms. This style of analysis would be especially powerful in cases where AIM is being used to analyze morphometry of specific regions of a priori interest.

Spatial Permutation Testing. We test for correspondence between cortical maps using the previously described spatial permutation ("spin") approach (26, 72), as implemented by Vasa et al. (6) for the 308-region parcellation (https://github.com/frantisekvasa/rotate_parcellation). We first obtained the coordinates of each of 308 regions on the Freesurfer spherical projection of the parcellation (using the fsaverage brain surface). These coordinates were then rotated about the three principal axes at randomly generated angles θx, θy, and $\theta z \in [0, 2p)$, with the following rotation matrices:

$$R_x(\theta) = \begin{matrix} 1 & 0 & 0 \\ 0 & \cos(\theta) & -\sin(\theta) \\ 0 & \sin(\theta) & \cos(\theta) \end{matrix}, \quad R_y(\theta) = \begin{matrix} \cos(\theta) & 0 & \sin(\theta) \\ 0 & 1 & 0 \\ -\sin(\theta) & 0 & \cos(\theta) \end{matrix},$$

$$R_z(\theta) = \begin{matrix} \cos(\theta) & -sin(\theta) & 0 \\ \sin(\theta) & \cos(\theta) & 0 \\ 0 & 0 & 1 \end{matrix}$$

Given the separate hemisphere surface projections, the rotation was applied to both hemispheres. To maintain hemispheric symmetry, the same random angles were used for both hemispheres, except that the sign of the angles was flipped for the rotations around the y and z axes (i.e., $\theta yR = -\theta yL$ and $\theta zR = -\theta zL$ but $\theta xL = \theta xR$). Following rotation of the sphere, coordinates of the rotated regions were matched to coordinates of the initial regions by Euclidean distance, proceeding in a descending order of average pairwise Euclidean distance on the rotated and unrotated spheres (i.e., starting with the rotated region that is furthest away, on average, from the unrotated regions). The matching then provides a mapping from the set of regions to itself, allowing any regional measure to be permuted while preserving spatial contiguity and hemispheric symmetry.

Enrichment Analyses. Alexander-Bloch et al. (26) presented methods for assessing several questions relating to correspondence of brain maps, including brainwide comparisons of discrete maps ("Do these maps have a significantly similar spatial distribution?") and parcel-wise comparison of discrete maps ("Does parcel X from parcellation A significantly overlap with parcel Y from parcellation B?"). We extend these methods to assess the enrichment of signal from a continuous map in particular parcels (i.e., "Is anatomical imbalance decline with age enriched in this functional network?") and provide an interpretable quantitative metric for enrichment.

Consider two cortical maps, where, for a region i:

1) One map contains continuous statistical parameters β_i
2) One map contains discrete functional network assignments net(i). (This is easily replaceable with any discrete map.)

The enrichment of map 1 in functional network m is given by the following:

$$Enrichment_m = \frac{\sum_{net_i=m} \beta_i}{\frac{\sum_i \beta_i}{\frac{\#(net_i=m)}{\max(i)}}}.$$

The enrichment statistic captures whether the proportion of continuous signal observed in network m exceeds that which is expected from the size of network m. Significance of enrichment can be assessed by spatial permutation (Spatial Permutation Testing) and recomputing of enrichment to create a null distribution.

Lifespan Analysis. For the lifespan analysis (Fig. 4), we harmonized raw cortical thickness estimates across cohort using ComBAT (28), available at https://github.com/Jfortin1/ComBatHarmonization. Briefly, ComBAT uses an empirical Bayes algorithm to correct for both site-specific offsets in CT estimates as well as site-specific scaling effects. We used ComBAT to remove cohort effects while preserving effects of age (our key variable of interest) and sex (because sex composition differs between cohorts). After harmonization, we computed anatomical imbalance separately in each cohort, performing cohort-wise correction of CT estimates for age, sex, and Euler number as described above. Because ComBAT accounted for site differences, we did not correct for site at this stage.

We modeled the lifespan trajectory of anatomical imbalance across all participants in the harmonized dataset using penalized regression splines with the following model, as implemented in the R package *gamm4*:

$$\text{Average anatomical imbalance} \sim \text{s(age)}.$$

We fit an additional model to confirm that observed age effects survive covariation for sex, Euler number, and cohort:

$$\text{Average anatomical imbalance} \sim \text{s(age)} + \text{sex} + \text{Euler number} + \text{cohort}.$$

Twin Analysis. ABCD is a large longitudinal study designed to investigate the influence of genetic and environmental factors on neurodevelopment and health in childhood and adolescence (73, 74). A total of 11,878 children (ages 9 through 10 y) and their parents were recruited across 21 sites in the United States. Notably, a substudy of ~800 pairs of same-sex twins was included within the ABCD cohort (75). All participants provided informed consent (parent) and assent (child), provided DNA samples for genotyping, completed a myriad of questionnaires and tasks, and completed an MRI protocol. Following the exclusions described below, the final analytic sample in the present study consisted of 348 monozygotic twin pairs (49.71% female, mean age = 10.15 y). We computed anatomical imbalance separately in the set of twins with lower birthweight and the set of twins with higher birthweight. A total of 256 of these 348 twin pairs (48.05% female, mean age = 10.13 y) had available birthweight estimates where birthweight was unequal between cotwins and passed imaging quality control (QC) measures described in the main text (Euler number < 217, mean anatomical imbalance less than 4 SDs away from cohort mean).

Biological samples obtained from the ABCD cohort were processed by the Rutgers University Cell and DNA Repository, where the Affymetrix NIDA Smokescreen genotyping array (76) was used to assay ~700,000 single nucleotide polymorphisms (SNPs) (77). Preliminary quality control procedures performed by the original ABCD investigators pruned the number of variants to 517,724 SNPs. These minimally processed genotypes for 10,627 participants were then made available via the National Institute of Mental Health Data Archive as part of ABCD Release 2.0.1. In the present study, we followed best practices and used PLINK version 2.00 (78) to apply additional quality control procedures prior to estimating kinship. We first excluded 141 samples who were missing 5% or more of their genotype calls. We then applied standard thresholds to the typed variants, which resulted in the exclusion of i) 26,242 variants that were missing in more than 2% of individuals, ii) 90,837 variants with a Hardy–Weinberg Equilibrium $P < 1 \times 10^{-6}$, and iii) 49,986 variants due to a minor allele frequency less than 0.01.

Following quality control procedures, we used the KING-robust kinship estimator in PLINK version 2.00 to estimate kinship in the ABCD cohort. As we sought to first identify all pairs of first-degree relatives, we excluded all

pairs with a kinship coefficient less than 0.177. We then excluded pairs if their parent did not endorse the twin identification item in surveys, if they were discrepant for age, or if they were discrepant for sex. Zygosity was then inferred from the kinship coefficient (79), where 348 pairs with an estimate > 0.354 were identified as monozygotic twins and 474 pairs with an estimate between 0.177 and 0.354 were identified as dizygotic twins. For the purposes of the present study, only monozygotic twins were retained.

Data Availability. NIH data are available at https://nda.nih.gov/edit_collection.html?id=3142. PNC morphometric estimates used for this analysis are available at https://github.com/KirstieJane/NSPN_WhitakerVertes_PNAS2016. Data from the ABIDE project are available at http://fcon_1000.projects.nitrc.org/indi/abide/, HCP data are available at https://db.humanconnectome.org/. UK Biobank data are available at https://www.ukbiobank.ac.uk. Cam-CAN data are available at https://www.cam-can.org/index.php?content=dataset. ABCD data are available at https://nda.nih.gov/abcd.

ACKNOWLEDGMENTS. We thank 1) all participants and families who contributed data to the cohorts used, 2) František Váša and David Gruskin for insightful discussion and helpful comments on this manuscript, and 3) Allysa Warling for assistance with IQ analyses. A.N. is supported by Award Number T32GM007753 from the National Institute of General Medical Sciences. The content is solely the responsibility of the authors and does not necessarily represent the official views of the National Institute of General Medical Sciences or the NIH. This study was supported by the intramural research program of the National Institute of Mental Health (project funding: 1ZIAMH002949-03, clinical trials identifier: NCT00001246, protocol: 89-M-0006). E.T.B. is a National Institutes of Health Research Senior Investigator.

1. A. Alexander-Bloch, J. N. Giedd, E. Bullmore, Imaging structural co-variance between human brain regions. *Nat. Rev. Neurosci.* **14**, 322–336 (2013).
2. C. P. Klingenberg, Studying morphological integration and modularity at multiple levels: Concepts and analysis. *Philos. Trans. R. Soc. Lond. B Biol. Sci.* **369**, 20130249 (2014).
3. B. Hallgrímsson *et al.*, Deciphering the palimpsest: Studying the relationship between morphological integration and phenotypic covariation. *Evol. Biol.* **36**, 355–376 (2009).
4. A. R. Palmer, C. Strobeck, FLUCTUATING ASYMMETRY: Measurement, analysis, patterns. *Annu. Rev. Ecol. Syst.* **17**, 391–421 (1986).
5. J. P. Lerch *et al.*, Studying neuroanatomy using MRI. *Nat. Neurosci.* **20**, 314–326 (2017).
6. F. Váša *et al.*; NSPN consortium, Adolescent tuning of association cortex in human structural brain networks. *Cereb. Cortex* **28**, 281–294 (2018).
7. B. A. Zielinski, E. D. Gennatas, J. Zhou, W. W. Seeley, Network-level structural covariance in the developing brain. *Proc. Natl. Acad. Sci. U.S.A.* **107**, 18191–18196 (2010).
8. B. S. Khundrakpam *et al.*; Brain Development Cooperative Group, Developmental changes in organization of structural brain networks. *Cereb. Cortex* **23**, 2072–2085 (2013).
9. H. Grydeland *et al.*, Waves of maturation and senescence in micro-structural MRI markers of human cortical myelination over the lifespan. *Cereb. Cortex* **29**, 1369–1381 (2019).
10. G. Douaud *et al.*, A common brain network links development, aging, and vulnerability to disease. *Proc. Natl. Acad. Sci. U.S.A.* **111**, 17648–17653 (2014).
11. C. K. Tamnes *et al.*; Alzheimer's Disease Neuroimaging Initiative, Brain development and aging: Overlapping and unique patterns of change. *Neuroimage* **68**, 63–74 (2013).
12. B. Hallgrímsson, K. Willmore, B. K. Hall, Canalization, developmental stability, and morphological integration in primate limbs. *Am. J. Phys. Anthropol.* **35** (suppl. 35), 131–158 (2002).
13. G. C. Banks, J. H. Batchelor, M. A. McDaniel, Smarter people are (a bit) more symmetrical: A meta-analysis of the relationship between intelligence and fluctuating asymmetry. *Intelligence* **38**, 393–401 (2010).
14. J. E. Schmitt *et al.*, Variance decomposition of MRI-based covariance maps using genetically informative samples and structural equation modeling. *Neuroimage* **47**, 56–64 (2009).
15. A. Alexander-Bloch, A. Raznahan, E. Bullmore, J. Giedd, The convergence of maturational change and structural covariance in human cortical networks. *J. Neurosci.* **33**, 2889–2899 (2013).
16. A. Raznahan *et al.*, Patterns of coordinated anatomical change in human cortical development: A longitudinal neuroimaging study of maturational coupling. *Neuron* **72**, 873–884 (2011).
17. R. Romero-Garcia *et al.*; NSPN Consortium, Structural covariance networks are coupled to expression of genes enriched in supragranular layers of the human cortex. *Neuroimage* **171**, 256–267 (2018).
18. Y. Yee *et al.*, Structural covariance of brain region volumes is associated with both structural connectivity and transcriptomic similarity. *Neuroimage* **179**, 357–372 (2018).
19. A. Sotiras *et al.*, Patterns of coordinated cortical remodeling during adolescence and their associations with functional specialization and evolutionary expansion. *Proc. Natl. Acad. Sci. U.S.A.* **114**, 3527–3532 (2017).
20. N. R. Lee *et al.*, Anatomical coupling among distributed cortical regions in youth varies as a function of individual differences in vocabulary abilities. *Hum. Brain Mapp.* **35**, 1885–1895 (2014).
21. W. W. Seeley, R. K. Crawford, J. Zhou, B. L. Miller, M. D. Greicius, Neurodegenerative diseases target large-scale human brain networks. *Neuron* **62**, 42–52 (2009).
22. D. S. Bassett *et al.*, Hierarchical organization of human cortical networks in health and schizophrenia. *J. Neurosci.* **28**, 9239–9248 (2008).
23. R. J. Jirsaraie *et al.*, Accelerated cortical thinning within structural brain networks is associated with irritability in youth. *Neuropsychopharmacology* **44**, 2254–2262 (2019).
24. R. A. I. Bethlehem, R. Romero-Garcia, E. Mak, E. T. Bullmore, S. Baron-Cohen, Structural covariance networks in children with autism or ADHD. *Cereb. Cortex* **27**, 4267–4276 (2017).
25. A. F. G. Rosen *et al.*, Quantitative assessment of structural image quality. *Neuroimage* **169**, 407–418 (2018).
26. A. F. Alexander-Bloch *et al.*, On testing for spatial correspondence between maps of human brain structure and function. *Neuroimage* **178**, 540–551 (2018).
27. B. T. T. Yeo *et al.*, The organization of the human cerebral cortex estimated by intrinsic functional connectivity. *J. Neurophysiol.* **106**, 1125–1165 (2011).
28. J.-P. Fortin *et al.*, Harmonization of cortical thickness measurements across scanners and sites. *Neuroimage* **167**, 104–120 (2018).
29. A. M. Fjell *et al.*, Development and aging of cortical thickness correspond to genetic organization patterns. *Proc. Natl. Acad. Sci. U.S.A.* **112**, 15462–15467 (2015).
30. J. E. Moodie *et al.*, Fluctuating asymmetry in brain structure and general intelligence in 73-year-olds. *Intelligence* **78**, 101407 (2020).
31. S. Ritchie, *Intelligence: All That Matters* (John Murray Press, 2015).
32. A. Raznahan, D. Greenstein, N. R. Lee, L. S. Clasen, J. N. Giedd, Prenatal growth in humans and postnatal brain maturation into late adolescence. *Proc. Natl. Acad. Sci. U.S.A.* **109**, 11366–11371 (2012).
33. T. L. Jernigan, S. A. Brown, G. J. Dowling, The adolescent brain cognitive development study. *J. Res. Adolesc.* **28**, 154–156 (2018).
34. C. H. Waddington, *The Strategy of the Genes* (Routledge, 2014).
35. C. H. Waddington, Canalization of development and the inheritance of acquired characters. *Nature* **150**, 563–565 (1942).
36. L. M. Rimol *et al.*, Cortical thickness is influenced by regionally specific genetic factors. *Biol. Psychiatry* **67**, 493–499 (2010).
37. K. L. Grasby *et al.*, Alzheimer's Disease Neuroimaging Initiative; CHARGE Consortium; EPIGEN Consortium; IMAGEN Consortium; SYS Consortium; Parkinson's Progression Markers Initiative; Enhancing NeuroImaging Genetics through Meta-Analysis Consortium (ENIGMA)—Genetics working group, The genetic architecture of the human cerebral cortex. *Science* **367**, eaay6690 (2020).
38. J. E. Schmitt, J. N. Giedd, A. Raznahan, M. C. Neale, The genetic contributions to maturational coupling in the human cerebrum: A longitudinal pediatric twin imaging study. *Cereb. Cortex* **28**, 3184–3191 (2018).
39. J. Teeuw *et al.*, Genetic influences on the development of cerebral cortical thickness during childhood and adolescence in a Dutch longitudinal twin sample: The brainscale study. *Cereb. Cortex* **29**, 978–993 (2019).
40. N. Gogtay *et al.*, Dynamic mapping of human cortical development during childhood through early adulthood. *Proc. Natl. Acad. Sci. U.S.A.* **101**, 8174–8179 (2004).
41. R. L. Buckner, F. M. Krienen, The evolution of distributed association networks in the human brain. *Trends Cogn. Sci.* **17**, 648–665 (2013).
42. A. Etkin, T. D. Wager, Functional neuroimaging of anxiety: A meta-analysis of emotional processing in PTSD, social anxiety disorder, and specific phobia. *Am. J. Psychiatry* **164**, 1476–1488 (2007).
43. A. Anticevic *et al.*, The role of default network deactivation in cognition and disease. *Trends Cogn. Sci.* **16**, 584–592 (2012).
44. G. E. Doucet *et al.*, Transdiagnostic and disease-specific abnormalities in the default-mode network hubs in psychiatric disorders: A meta-analysis of resting-state functional imaging studies. *Eur. Psychiatry* **63**, e57 (2020).
45. N. Raz, "Aging of the brain and its impact on cognitive performance: Integration of structural and functional findings" in *The Handbook of Aging and Cognition* (Lawrence Erlbaum Associates Publishers, ed. 2, 2000), vol. 2, pp. 1–90.
46. F. Chouinard-Decorte *et al.*, Heritable changes in regional cortical thickness with age. *Brain Imaging Behav.* **8**, 208–216 (2014).
47. W. Jagust, Imaging the evolution and pathophysiology of Alzheimer disease. *Nat. Rev. Neurosci.* **19**, 687–700 (2018).
48. M. Saggar *et al.*, Estimating individual contribution from group-based structural correlation networks. *Neuroimage* **120**, 274–284 (2015).
49. K. M. Abel *et al.*, Birth weight, schizophrenia, and adult mental disorder: Is risk confined to the smallest babies? *Arch. Gen. Psychiatry* **67**, 923–930 (2010).
50. M. Horikoshi *et al.*, Meta-Analyses of Glucose- and Insulin-related traits Consortium (MAGIC); Early Growth Genetics (EGG) Consortium, New loci associated with birth weight identify genetic links between intrauterine growth and adult height and metabolism. *Nat. Genet.* **45**, 76–82 (2013).
51. E. DuPre, R. N. Spreng, Structural covariance networks across the life span, from 6 to 94 years of age. *Netw. Neurosci.* **1**, 302–323 (2017).
52. Manu *et al.*, Canalization of gene expression and domain shifts in the Drosophila blastoderm by dynamical attractors. *PLoS Comput. Biol.* **5**, e1000303 (2009).
53. G. Huelsz-Prince, J. S. van Zon, Canalization of C. elegans vulva induction against anatomical variability. *Cell Syst.* **4**, 219–230.e6 (2017).
54. Manu *et al.*, Canalization of gene expression in the Drosophila blastoderm by gap gene cross regulation. *PLoS Biol.* **7**, e1000049 (2009).
55. J. P. Lerch *et al.*, Mapping anatomical correlations across cerebral cortex (MACACC) using cortical thickness from MRI. *Neuroimage* **31**, 993–1003 (2006).
56. K. L. Miller *et al.*, Multimodal population brain imaging in the UK Biobank prospective epidemiological study. *Nat. Neurosci.* **19**, 1523–1536 (2016).

57. A. Raznahan *et al*., How does your cortex grow? *J. Neurosci.* **31**, 7174–7177 (2011).
58. N. U. F. Dosenbach *et al*., Real-time motion analytics during brain MRI improve data quality and reduce costs. *Neuroimage* **161**, 80–93 (2017).
59. T. S. Coalson, D. C. Van Essen, M. F. Glasser, The impact of traditional neuroimaging methods on the spatial localization of cortical areas. *Proc. Natl. Acad. Sci. U.S.A.* **115**, E6356–E6365 (2018).
60. A. M. Dale, B. Fischl, M. I. Sereno, Cortical surface-based analysis. I. Segmentation and surface reconstruction. *Neuroimage* **9**, 179–194 (1999).
61. B. Fischl, A. Liu, A. M. Dale, Automated manifold surgery: constructing geometrically accurate and topologically correct models of the human cerebral cortex. *IEEE Trans Med Imaging* **20**, 70–80 (2001).
62. F. Ségonne, J. Pacheco, B. Fischl, Geometrically accurate topology-correction of cortical surfaces using nonseparating loops. *IEEE Trans Med Imaging* **26**, 518–529 (2007).
63. B. Fischl *et al*., Sequence-independent segmentation of magnetic resonance images. *Neuroimage* **23 Suppl 1**, S69–S84 (2004).
64. B. Fischl, A. M. Dale, Measuring the thickness of the human cerebral cortex from magnetic resonance images. *Proc Natl Acad Sci U S A* **97**, 11050–11055 (2000).
65. X. Han *et al*., Reliability of MRI-derived measurements of human cerebral cortical thickness: the effects of field strength, scanner upgrade and manufacturer. *Neuroimage* **32**, 180–194 (2006).
66. B. Fischl, M. I. Sereno, A. M. Dale, Cortical surface-based analysis. II: Inflation, flattening, and a surface-based coordinate system. *Neuroimage* **9**, 195–207 (1999).
67. M. Reuter, N. J. Schmansky, H. D. Rosas, B. Fischl, Within-subject template estimation for unbiased longitudinal image analysis. *Neuroimage* **61**, 1402–1418 (2012).
68. An automated labeling system for subdividing the human cerebral cortex on MRI scans into gyral based regions of interest. *Neuroimage* **31**, 968–980 (2006).
69. R. Romero-Garcia, M. Atienza, L. H. Clemmensen, J. L. Cantero, Effects of network resolution on topological properties of human neocortex. *Neuroimage* **59**, 3522–3532 (2012).
70. K. J. Whitaker *et al*., NSPN Consortium, Adolescence is associated with genomically patterned consolidation of the hubs of the human brain connectome. *Proc Natl Acad Sci U S A* **113**, 9105–9110 (2016).
71. N. Weiskopf *et al*., Quantitative multi-parameter mapping of R1, PD(*), MT, and R2(*) at 3T: a multi-center validation. *Front Neurosci* **7**, 95 (2013).
72. S. N. Vandekar *et al*., Topologically dissociable patterns of development of the human cerebral cortex. *J Neurosci* **35**, 599–609 (2015).
73. N. D. Volkow *et al*., The conception of the ABCD study: From substance use to a broad NIH collaboration. *Dev Cogn Neurosci* **32**, 4–7 (2018).
74. H. Garavan *et al*., Recruiting the ABCD sample: Design considerations and procedures. *Dev Cogn Neurosci* **32**, 16–22 (2018).
75. W. G. Iacono *et al*., The utility of twins in developmental cognitive neuroscience research: How twins strengthen the ABCD research design. *Dev Cogn Neurosci* **32**, 30–42 (2018).
76. J. W. Baurley, C. K. Edlund, C. I. Pardamean, D. V. Conti, A. W. Bergen, Smokescreen: a targeted genotyping array for addiction research. *BMC Genomics* **17**, 145 (2016).
77. K. A. Uban *et al*., Adolescent Brain Cognitive Development Study, Biospecimens and the ABCD study: Rationale, methods of collection, measurement and early data. *Dev Cogn Neurosci* **32**, 97–106 (2018).
78. C. C. Chang *et al*., Second-generation PLINK: rising to the challenge of larger and richer datasets. *Gigascience* **4**, 7 (2015).
79. A. Manichaikul *et al*., Robust relationship inference in genome-wide association studies. *Bioinformatics* **26**, 2867–2873 (2010).